IEEE Access
Multidisciplinary ⋮ Rapid Review ⋮ Open Access Journal

Study on the automatic segmentation of metal source applicators in after-loading treatment of cervical cancer patients based on the U-Net

Lingyun Qiu1, Rong Wu2⸸, Xinpeng Lin3, Lifeng Qiu4, Kainan Shao1, Wenming Zhan1, Qiang Li1, Jieni Ding1, Yucheng Li1⸸, Weijun Chen1*

[1]Cancer Center, Department of Radiation Oncology, Zhejiang Provincial People's Hospital, Affiliated People's Hospital, Hangzhou Medical College, Hangzhou, Zhejiang, China.
[2]Department of Breast Surgery, Hangzhou Hospital of Traditional Chinese Medicine, 453 Tiyuchang Road, Hangzhou, Zhejiang Province, China.
[3]Department of Medical Imaging, Hangzhou Medical College, Hangzhou, Zhejiang, China.
[4]Department of Oncology, Guangxi Medical University Kaiyuan Langdong Hospital, No 60 Jinhu North Road, Nanning 530028, Guangxi, China.

Corresponding author: Weijun Chen (e-mail: chenweijun@hmc.edu.cn).

⸸these authors contributed equally to this work
"This work was supported in part by the Zhejiang Province Natural Science Foundation of China under Grant No. LGF21H180014 and the Medical and Health Research Project of Zhejiang Province under Grant No.2021PY002. Thanks to MANTEIA for technical support. Thanks to American Journal Expert for help with language editing."

ABSTRACT This study utilized the U-Net deep learning model to automate the segmentation of three-dimensional after-loaded metal source applicators, aiming to expedite treatment planning, reduce patient wait times, and enhance the treatment process. Using CT images from cervical cancer patients treated between December 2020 and August 2023, 27 images formed the training set, 3 were for validation, and 10 for testing. The model's performance was evaluated against expert delineations using metrics like the Dice similarity coefficient (DSC), Hausdorff distance 95% (HD95), and others. The results were integrated into a after-loading planning system to locate applicator pathways and assess dose accuracy and feasibility. For the test group, the DSC ranged from 0.90 to 0.93, HD95 from 0.79 to 0.80 mm, and ASSD from 0.03 to 0.22 mm, with an average segmentation time of 65 seconds, significantly faster than manual delineation. The automatic pathways closely matched the original plan's dosimetric parameters ($P > 0.05$), indicating the system's potential for safe application in after-loading planning for cervical cancer treatment. The U-Net-based region-growing method shows promise in improving the efficiency and accuracy of after-loaded applicator segmentation.

Keywords: Cervical cancer, After-loaded treatment planning, Deep learning, U-Net, Automatic segmentation.

I. INTRODUCTION

Cervical cancer is a common gynecological malignancy worldwide and is characterized by a high incidence and significant threat to patient health, making it a focal point for the World Health Organization (WHO) [1]. According to data from the WHO, in 2020, there were approximately 604,000 new cases of cervical cancer worldwide, with 342,000 deaths; cervical cancer was thus the fourth most common cancer by incidence [2]. Radiotherapy plays a crucial role in the treatment of cervical cancer, and after-loading treatment is an indispensable portion of radiotherapy [3], [4].

Traditional after-loading treatment for cervical cancer typically involves two-dimensional planning, which is a widely used method. However, with the continuous advancement of medical technology, three-dimensional after-loading treatment plans have gained increasing attention. Compared to traditional two-dimensional planning, three-dimensional after-loading treatment offers a range of significant advantages, including greater precision, personalized treatment, treatment monitoring, and reduced side effects [5], [6], [7]. However, three-dimensional after-loading treatment also has several limitations. For example, this process requires target area delineation and source applicator reconstruction; these processes often require a significant amount of time and human resources [8]. Using AI for target area delineation is difficult due to individual patient variations. However, using AI for source applicator reconstruction is more feasible for AI automation because their shape is generally fixed, and the tissue density differs from that of human tissue, especially for metal source applicators [9], [10], [11]. Currently, there are relatively few reports on the automatic segmentation of cervical cancer after-loading source applicators using the U-Net algorithm [12].

In this study, a neural network region-growing deep learning (DL) model based on a small-sample U-Net training set was proposed. The proposed model was trained and evaluated for the automatic segmentation of metal source applicators in after-loading simulated CT images of cervical cancer patients. Subsequently, the performance of the DL algorithm model was compared against that of traditional manual delineation methods using software. Additionally, post processing of the source applicators was performed through skeletonization and polynomial curve fitting. The automatic reconstruction of source applicator pathways was achieved in the three-dimensional after-loading planning system, and the accuracy of the study results was assessed using dosimetric evaluation methods.

Materials and Methods

Data and data annotation

The study was approved by the Medical Ethics Committee of Zhejiang Provincial People's Hospital (2024-03-11, No. QT2024054). Due to the retrospective nature of the analysis, the requirement for informed consent was waived. Data for this retrospective analysis were collected and analyzed between November 2023 and January 2024. The patient data was completely anonymous, and during or after data collection, the authors could not obtain information that could identify individual participants.

In this article, the localization CT imaging data of 40 patients who underwent cervical cancer after-loading brachytherapy at our institution from December 2020 to August 2023 were retrospectively studied. The CT images had a resolution of 0.1 cm × 0.1 cm × 0.3 cm, with a range of 37 to 65 slices and an average of 54 slices. The age of the 40 patients ranged from 32 to 87 years, with a median age of 54.5 years. The body mass index (BMI) ranged from 18 to 25, with a median value of 21.

The inclusion criteria for patients were as follows: ① Had early-stage cervical cancer after surgery, where this cancer was clinically staged as T1-2N0M0, and lacked distant metastasis. ② The absence of other systemic diseases. The exclusion criteria for patients were as follows: ① Had contraindications to radiotherapy. ② Previously received radiotherapy, chemotherapy, or other antitumor treatments.

All 40 cases included metal tube applicators (Xinhua applicator, Shandong, No. 084.350). The applicators on the CT images were contoured by experienced physicists using the Acclearning platform (Manteia, Xiamen, China). High-level physicists manually delineated the contours containing the applicators in the CT images and labeled the three applicators as Source_L, Source_M, and Source_R, representing the left, middle, and right applicators, respectively.

Data preprocessing

The training set's CT images were subjected to Z score normalization, which involved subtracting the dataset's image mean from each data point and then dividing that difference by the standard deviation. This normalization ensures data quality and consistency while enhancing the contrast between the source applicators and the backgrounds of the images, emphasizing the applicator features. After preprocessing, voxel resampling was applied to the images, uniformly resampling them to a voxel size of 1.0×1.0 while maintaining the slice thickness. Since source applicators are typically located in the middle portion of CT images, random window cropping was performed on the CT images and their corresponding ground truth images. The window center was randomly selected from the ground truth and background images at a 1:1 ratio, and the window size was set to 320×320. To increase the dataset diversity, data augmentation techniques, including flipping, scaling, rotation, gamma transformation, and elastic deformation, were applied to the training images. Both window sampling and data augmentation were performed online during the training phase to achieve the best augmentation results.

Construction of the U-Net model

Construction of the network model

We employed a medical image segmentation network architecture based on U-Net, which consists of a total of 10 parts. The model takes the input as 320×320 CT images. The first 5 layers are downsampling layers, each comprising two convolution operations and one max pooling operation. Layers 6 to 9 are upsampling layers; after a deconvolution operation in each layer, low-level and high-level information are fused through skip connection layers, enabling the model to capture both semantic information and textural details. Subsequently, two convolution operations are performed, with a convolution kernel size of 3×3, a deconvolution kernel size and a max pooling kernel size of 2×2, and a stride of 1. The activation function used was the rectified linear unit (ReLU). In the 10th layer, cross-channel features are integrated using a 1×1 convolutional kernel with the sigmoid activation function, resulting in a final output of a 320×320 two-dimensional prediction map (as shown in Figure 1).

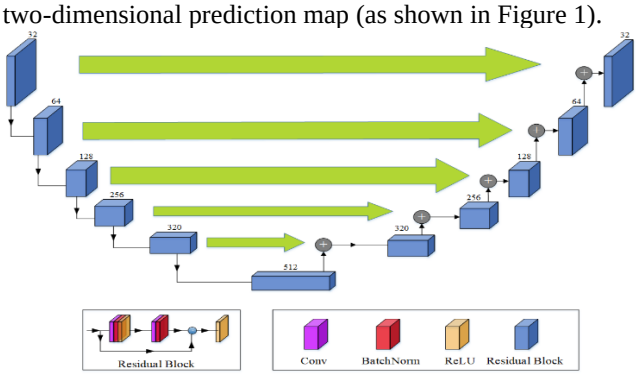

Figure 1. The structure of U-net network

annotation: Conv: Convolutional Layer, BatchNorm: Batch Normalization Layer, ReLU, Residual Block: Residual Connection Block

Model optimization

The optimizer optimized during training is Adam (adaptive moment estimation) [13]. Adam dynamically adjusts the learning rate for each parameter using first and second-order moment estimates of the gradients. After bias correction, the learning rate is within a determined range

after each iteration, ensuring parameter integrity. The selected loss function is a combination of cross-entropy and Dice loss [14].

Training and segmentation of the network

The preprocessed training and validation sets are fed into the network for training with a batch size of 8. For each batch of data, the model's forward propagation process calculates the model's output. The input images are mapped to segmentation masks indicating the positions of the metal source applicators. The difference between the segmentation mask generated by the model and the real label mask (from the training set) is computed to determine the loss. This loss represents measures the discrepancy between the model's output and ground truth. Using the computed loss, gradients are calculated using the backpropagation algorithm to determine how each model parameter affects the loss. An optimizer is used to update the model's weights and biases to minimize the loss through self-adjustment. After each training epoch, the model's performance is evaluated using the validation set. The maximum number of epochs is set to 200, the initial learning rate is set to 3^{e-4}, and the exponential moving average loss is calculated for both the training and validation sets. If the loss does not decrease by more than 1% within 3 epochs, the learning rate is reduced by 50%. To improve the model's performance, the hyperparameters are adjusted based on the performance on the validation set. Training ends when the validation set performance no longer improves. Once training is complete and the model's performance stabilizes with an increasing number of samples (as shown in Figure 2), the test set data are input into the network for segmentation. This process yields the segmentation results for each patient, which are subsequently evaluated, including the Dice index, to assess the model's performance.

Figure 2. Evolution of Dice similarity coefficient (DSC) of train and validation data sets during the training process.

annotation: loss_tr: training set loss curve, loss_val: validation set loss curve, pseudo dice: validation set pseudo dice curve, pseudo dice (mov. avg.): moving average of validation set pseudo dice curve.

Model evaluation

The accuracy of source applicator reconstruction depends on the segmentation accuracy of the applicators. Therefore, to assess segmentation effectiveness, the following seven metrics are adopted for evaluation [13], [15], [16].

DSC

The compilation section of the model defines the DSC, which is used to measure the similarity between two samples and has values ranging from 0 to 1. A value of 0 represents dissimilarity, while 1 indicates a high degree of similarity and excellent segmentation results. In actual predictions, each patient has CT images comprising 70-90 layers. Therefore, the mean and standard deviation of the DSC are calculated; the same approach is used for all other evaluations.

Hausdorff distance (HD)

Since the DSC is sensitive to the internal filling ratio, the HD is used to evaluate the model. Given two samples A and B in the spatial domain, the HD is used to measure the distance between these two samples. The HD is calculated as follows:

$$\mathrm{HD}(A,B) = \max\left(\mathrm{D}(A,B), \mathrm{D}(B,A)\right) \quad (1)$$

In the equation (1), $\mathrm{D}(A,B) = \max a \epsilon A \min b \epsilon B ||a-b||$, where A represents the predicted image, B represents the ground truth image, and a and b are elements within A and B, respectively. To account for outliers in both the predicted and ground truth images, the 95th percentile of the HD is computed and denoted as HD95.

Relative Volume Difference（RVD）

The RVD is defined as follows:

$$\mathrm{RVD} = \left(\frac{A+\lambda}{B+\lambda} - 1\right) \times 100 \quad (2)$$

Where λ is the Laplace smoothing factor. In the equation (2), λ is set to 1 to prevent division by zero.

Average Symmetric Surface Distance（ASSD）

The ASSD represents calculates the minimum Euclidean distance between all points in the predicted surface point set and the reference surface point set and then calculates the average of all these distances, where 0 is the best value, and infinity is the worst.

Relative Absolute Volume Difference (RAVD)

The RAVD calculates the relative coefficient of the nonoverlapping portions of the predicted volume and the reference volume, where 0% is the best value, and infinity is the worst.

Jaccard Similarity Coefficient（Jaccard）

The Jaccard similarity coefficient compares the elements of two sets to determine which elements overlap and which do not. This measures the similarity between two sets of data, where 1.0 is the best value, and 0 is the worst.

Centroid Distance (CD)

The CD between sets A and B is the average distance between the centroids of A and B. The CD is calculated by finding the average pairwise distance between points within each set, where 0 is the best value, and infinity is the worst.

Dosimetric evaluation

We applied the automated reconstruction of source catheter paths for the 10 test patients to the three-dimensional postimplantation treatment planning system. We duplicated the dwell positions and dwell times of each source applicator from the original clinical plan and used the original radioactive source activity to generate new test plans. Finally,

we identified the differences between the dosimetric parameters of the two sets of plans. The compared parameters included D90 (Gy) and D100 (Gy) for the HR-CTV (high-risk tumor region) and IR-CTV (low-risk tumor region), as well as V100 (%), V150 (%), and V200 (%) for these regions. Additionally, we evaluated D0.1 cc, D1 cc, and D2 cc for the rectum, bladder, and sigmoid colon. SPSS 19.0 software was used to perform paired t tests to assess the differences between the two sets of data.

Results

Model training results

After 25 epochs, the loss functions on the training and validation sets converged to lower levels. After 200 epochs, the training set loss decreased to 0.07, and the validation set loss decreased to 0.1. The training set exhibited a DSC of 0.93, while the validation set exhibited a DSC of 0.90, indicating that the model learned the features of the source applicators effectively. The total training time was 7 hours. The loss curves for the training and validation sets during the training process showed that the model converged after 200 epochs, as shown in Figure 2.

Figure 3 shows the comparison of the final evaluation parameters for the four source applicator models trained with 15, 20, 25, and 30 cases in the training set and validation set. The Dice values for the left, middle, and right applicators gradually increased as the number of training and validation cases increased, and eventually stabilized. The other evaluation parameters for the four different training and validation sets varied for the three applicators. Based on the comparison of the final evaluation results, the model trained with 30 cases in the training set and validation set was selected for further source applicator segmentation research. Table 1 lists the specific values of the final evaluation parameters for the source applicator models trained with 30 cases in the training set and validation set; the Dice values are slightly lower for the left applicator and greater for the middle and right applicators, averaging 0.91 and 0.89, respectively.

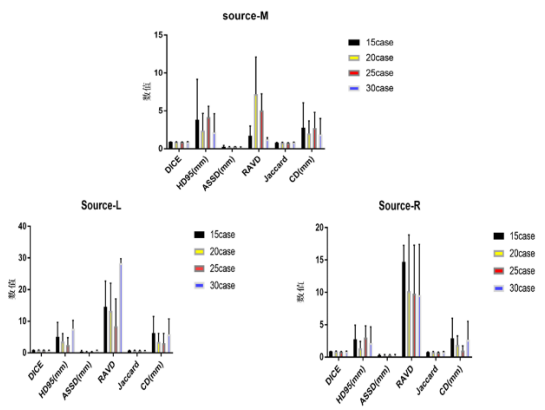

Figure 3. A bar chart depicting the evaluation parameters of the four source applicator models.

Table 1. Model evaluation parameter results for the validation set (x(s))

Roi	dice	hd95	assd	ravd	jaccard	cd
Source_L	0.81	7.60	0.58	28.39	0.68	5.84
	(0.02)	(2.15)	(0.19)	(1.13)	(0.02)	(3.97)
Source_M	0.91	2.15	0.15	1.21	0.84	1.86
	(0.01)	(2.02)	(0.09)	(0.21)	(0.02)	(1.74)
Source_R	0.89	2.17	0.23	9.60	0.80	2.70
	(0.03)	(2.04)	(0.15)	(6.38)	(0.05)	(2.30)
Mean	0.87	3.97	0.32	13.07	0.77	3.47
	(0.02)	(2.07)	(0.14)	(2.57)	(0.03)	(2.67)

The selected best trained model was used to segment the 10 patients in the test set. Taking the first patient as an example, the segmentation results of the source applicator obtained by using this model are stronger, as shown in Figure 4. Figure 5 illustrates the differences between the 3D contours of the source applicator trained by the model and the contours manually drawn by the experienced physicist.

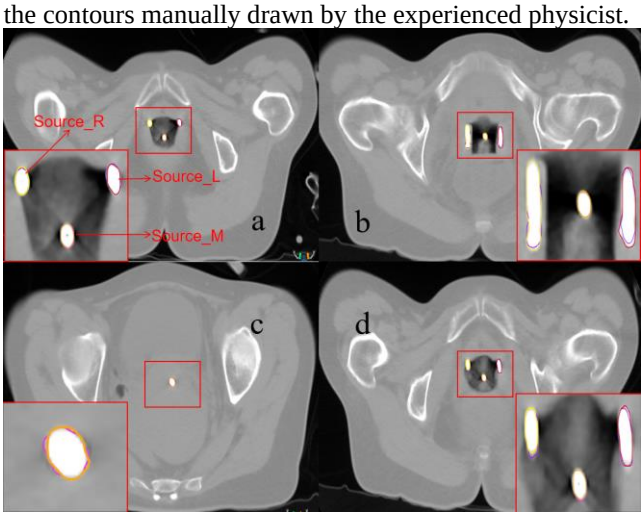

Figure 4. Comparison of the applicator Cross-sectional image predicted by U-net (blue) and the manual delineated (red) in patient 1

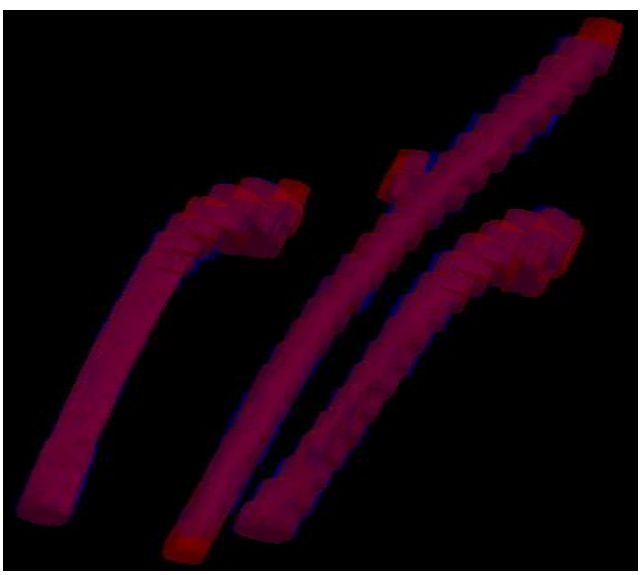

Figure 5. Comparison of the applicator 3d model predicted by U-net (blue) and the manual delineated (red) in patient 2

The segmentation results for the test set of 10 patients treated with metal cylinder applicators were satisfactory. Compared to the applicator contours manually delineated by experienced physicists, the average DSC for the left applicator is 0.91, the HD95 is 0.80 mm, the ASSD is 0.22 mm, the MSSD is 5.06 mm, and the RAVD is 6.26 mm. For the middle applicator, the average DSC is 0.90, the HD95 is 0.79 mm, the ASSD is 0.03 mm, the MSSD is 5.06 mm, and the RAVD is 1.19 mm. Finally, for the right applicator, the average DSC is 0.93, the HD95 is 0.79 mm, the ASSD is 0.20 mm, the MSSD is 5.06 mm, and the RAVD is 4.99 mm. The CT segmentation prediction time for these cases ranged from a minimum of 78 seconds to a maximum of 124 seconds, with an average of 88 seconds. The specific numerical values are provided in Tables 2, 3, and 4, and the corresponding bar chart is shown in Figure 6.

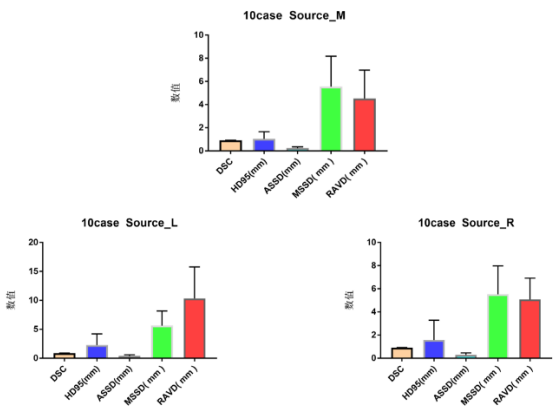

Figure 6. Bar chart of the evaluation parameters for the applicator test set of the model.

Table 2. The left applicator evaluation parameters of 10 patients test set

Patient Number	DSC	HD95(mm)	ASSD(mm)	MSSD(mm)
1	0.91	0.80	0.22	5.06
2	0.88	5.05	0.66	10.11
3	0.87	1.54	0.33	5
4	0.86	5.03	0.73	10.08
5	0.89	0.61	0.29	5.08
6	0.91	0.57	0.22	5.03
7	0.88	1.42	0.3	2.88
8	0.89	1.48	0.32	5.05
9	0.8	5	0.62	5.17
10	0.88	1.2	0.23	2.72
Mean	0.9	0.79	0.22	5.06

Table 3. The middle applicator evaluation parameters of 10 patients test set

Patient Number	DSC	HD95(mm)	ASSD(mm)	MSSD(mm)
1	0.9	0.79	0.29	5.06
2	0.91	0.74	0.36	10.03
3	0.93	0.77	0.06	1.54
4	0.89	1.59	0.4	10.08
5	0.92	0.62	0.16	5.08
6	0.93	0.57	0.13	5
7	0.87	1.42	0.29	5.05
8	0.91	0.74	0.2	5.05
9	0.92	0.59	0.16	5.04
10	0.87	2.5	0.32	3.62

Table 4. The right applicator evaluation parameters of 10 patients test set

Patient Number	DSC	HD95(mm)	ASSD(mm)	MSSD(mm)
1	0.93	0.79	0.2	5.06
2	0.87	5.05	0.67	10.11
3	0.89	1.09	0.28	5.06
4	0.92	0.56	0.24	5.25
5	0.9	0.62	0.26	5.04
6	0.92	0.8	0.19	5
7	0.91	1	0.17	2.5
8	0.89	1.05	0.29	5.05
9	0.88	5	0.57	10
10	0.93	0.54	0.12	2.56
Mean	0.93	0.79	0.2	5.06

Dosimetric evaluation results

As shown in Table 5, when comparing the dose metrics of the treatment plans reconstructed automatically by the model with the original plans for 10 cervical cancer patients, the p values (P) are all greater than 0.05. This indicates that the source paths automatically reconstructed by this model are reasonable and do not statistically significantly differ from the source contours manually drawn by experienced physicists. Detailed dose–volume histogram (DVH) comparisons for one of the patients are provided in Figure 7, illustrating minimal differences between the dose curves for organs at risk and the target area.

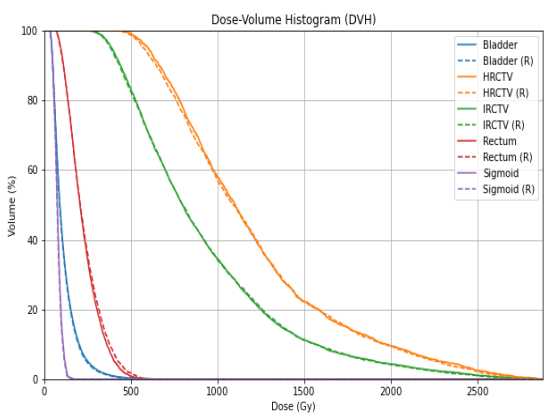

Figure 7. Comparison of DVH (Dose-Volume Histogram) for a Cervical Cancer.

Table 5. Comparison of Original Plans and Plans with Automatically Reconstructed Applicator Pathways for 10 Cervical Cancer Patients

annotation: Post plan: plan after reconstruction of the source applicator path

Project	Parameters	Original plan	Post plan	t value	p value
HR-CTV	D90(Gy)	690.04±39.17	673.53±37.71	1.348	0.211
	D100(Gy)	449.57±71.831	433.82±52.654	1.456	0.180
	V100(%)	88.59±4.388	87.22±3.93	1.280	0.232
	V150(%)	53.15±3.39	50.50±4.22	1.998	0.077
	V200(%)	30.42±3.41	28.62±2.75	2.230	0.053
IR-CTV	D90(Gy)	482.95±50.99	483.50±67.54	-0.086	0.934
	D100(Gy)	291.92±47.84	274.73±56.32	1.046	0.323
	V100(%)	63.13±8.95	60.79±9.73	1.263	0.238
	V150(%)	33.27±5.97	32.19±6.37	0.993	0.347
	V200(%)	19.58±3.56	18.63±4.39	1.094	0.303
Rectum	D0.1cc	506.20±92.78	499.50±102.08	0.321	0.756
	D1cc	402.07±87.29	404.15±104.79	-0.139	0.892
	D2cc	363.78±85.16	346.30±94.34	0.758	0.468
Bladder	D0.1cc	638.90±97.76	611.56±94.44	3.941	0.113
	D1cc	525.81±79.96	505.03±75.97	4.496	0.241
	D2cc	487.37±78.13	470.43±76.67	3.665	0.545
Sigmoid colon	D0.1cc	395.92±195.96	347.57±167.72	1.445	0.182
	D1cc	327.84±144.48	268.71±124.25	1.465	0.177
	D2cc	301.72±128.44	244.48±110.56	1.621	0.139

Discussion

In recent years, with the advancement of computer hardware, deep learning has been gradually improved in various fields, and different networks have been developed to solve various problems [17], [18]. In 2015, Ronneberger et al. [19] first introduced the U-Net, which is suitable for image segmentation with small datasets. It is designed for pixel-level classification and consists of an encoding and decoding part, with feature fusion achieved through skip connections. Due to its characteristics, U-Net has been widely applied in the medical image segmentation field [20]. Therefore, in this study, the U-Net network was chosen to combine deep learning technology with brachytherapy, enabling the source applicators in treatment planning to be rapidly and accurately reconstructed. This reduces the human errors introduced by physicists during the reconstruction process, resulting in more precise and convenient brachytherapy planning and ultimately enabling better treatment for patients.

Currently, limited research has been conducted on source applicator segmentation in brachytherapy. Zhang et al. [21] constructed an attention network and applied it to ultrasound-guided high-dose-rate prostate brachytherapy, successfully segmenting and locating the interstitial needles in ultrasound images. Zaffino et al. [15] used a three-dimensional U-Net network to reconstruct interstitial needles in MRI-guided cervical cancer brachytherapy, achieving a DSC of approximately 0.6. In comparison to these studies, our proposed method achieved a greater DSC. Furthermore, considering the high frequency of use of the three-tube source applicator at our institution, we specifically segmented and reconstructed the three-tube source applicator, improving the treatment effectiveness of our clinical practice.

The importance of the source applicator as a connection between the patient and the radiation source in brachytherapy is self-evident. The source applicator reconstruction quality plays a critical role in the entire treatment plan [22]. In this study, we constructed a model based on the U-Net framework, preprocessed CT images and ground truth maps and fed them into the model to allow it to learn the features of the source applicator. These learned features were subsequently applied to new cases. Through multiple evaluations of the model's segmentation results, we demonstrated the feasibility and reliability of this method, demonstrating that it can quickly and accurately segment the source applicator.

For 3D image-based brachytherapy (BT) in patients with cervical cancer who underwent postoperative radiotherapy, the dose calculation relies on the geometric accuracy of the source positions relative to the target volume and organs at risk (OAR). Due to the steep dose gradients in BT, uncertainties in source applicator positioning and reconstruction can lead to significant dose deviations between the target and OAR [23], [24], [25]. It has been demonstrated that a ±3 mm displacement of tandem and ovoid applicators or ±4.5 mm uncertainties in applicator reconstruction can result in dose variations of more than 10% in MRI-based BT for cervical cancer [26]. To minimize reconstruction uncertainties, avoid inadvertent errors, and achieve high precision and consistency, an automated source applicator reconstruction method with high accuracy is essential.

In our study, the automated source applicator reconstruction method based on the U-Net model achieved relatively high accuracy. The source applicator segmentation took only approximately 65 seconds, and the DSC accuracy reached 0.90. The selected model successfully segmented all source applicator contours in the 10-test set, with Dice values exceeding 0.9 and HD95 values less than 1 mm. The proposed model also achieved favorable numerical values on

other evaluation parameters, illustrating the high precision of the method used for source applicator reconstruction.

Automating after-loading treatment plan development is the future research direction. The planning process includes organ delineation, source applicator reconstruction, dose calculation, dose optimization, and plan evaluation [27]. We developed a after-loading treatment planning system (TPS) plugin tool in C++ that automatically converts source applicator contours into real source tube pathways. It can also automatically delineate organs at risk and target areas. The various dosimetric parameters of the automatically generated source tube pathways did not significantly differ ($P > 0.05$) from those of the manually planned pathways in the planning system. This finding first suggests that the proposed approach can be safely applied to three-dimensional after-loading treatment planning systems by dosimetric evaluation.

One of the limitations of this work is the relatively small size of the dataset. This limitation arises from the limited number of cervical cancer patients who underwent CT-based brachytherapy at our clinic. Increasing the size of the training dataset did not lead to a significantly improved Dice coefficient. Additionally, deep learning methods tend to benefit from larger datasets, which often yield improved performance and generalization. Therefore, we plan to collect more suitable image data in future research, and we expect to thereby achieve more accurate and reliable segmentation results.

To investigate the feasibility and accuracy of the proposed method, we began our research with relatively simple tandem and ovoid applicators. Therefore, this work can be considered an initial exploration and a simple test. Subsequent development and more comprehensive evaluation will be necessary to extend the proposed method to more challenging scenarios.

II. CONCLUSION

In this study, deep learning was utilized through the construction of a U-Net model and region growing to examine applicator reconstruction in brachytherapy treatment planning. The proposed model successfully segmented metal tube applicators, automatically recognizing their position and shape. The segmentation results were evaluated using various metrics, and the applicators were automatically incorporated into treatment planning software. The results demonstrated that the model achieved good segmentation performance, with favorable evaluation metric values. This approach is suitable for applicator reconstruction in clinical practice, and the resulting 3D brachytherapy plans can be preliminarily applied in clinical treatment. This research provides a new solution for applicator reconstruction in cervical cancer brachytherapy and has potential for widespread clinical adoption.

ACKNOWLEDGMENT

Thanks to MANTEIA for technical support. Thanks to American Journal Expert for help with language editing.

REFERENCES

[1] F. Bray, J. Ferlay, I. Soerjomataram, R. L. Siegel, L. A. Torre, and A. Jemal, "Global cancer statistics 2018: GLOBOCAN estimates of incidence and mortality worldwide for 36 cancers in 185 countries," *CA Cancer J Clin*, vol. 68, no. 6, 2018, doi: 10.3322/caac.21492.

[2] "World Health Organization (WHO). Human papillomavirus (HPV) and cervical cancer." Accessed: Dec. 11, 2023. [Online]. Available: https://www.who.int/en/news-room/fact-sheets/detail/human-papillomavirus-(hpv)-and-cervical-cancer

[3] C. Chargari *et al.*, "ESGO/ESTRO quality indicators for radiation therapy of cervical cancer," *International Journal of Gynecological Cancer*, vol. 33, no. 6, 2023, doi: 10.1136/ijgc-2022-004180.

[4] J. Chino *et al.*, "Radiation Therapy for Cervical Cancer: Executive Summary of an ASTRO Clinical Practice Guideline," *Pract Radiat Oncol*, vol. 10, no. 4, 2020, doi: 10.1016/j.prro.2020.04.002.

[5] X. Di *et al.*, "A new technique for trans-perirectal iodine-125 seed implantation in prostatic cancer guided by CT and 3D printed template: Two case reports," *Front Oncol*, vol. 12, 2022, doi: 10.3389/fonc.2022.1031970.

[6] J. Skowronek, "Current status of brachytherapy in cancer treatment – short overview," *J Contemp Brachytherapy*, vol. 9, no. 6, 2017, doi: 10.5114/jcb.2017.72607.

[7] A. E. Sturdza and J. Knoth, "Image-guided brachytherapy in cervical cancer including fractionation," *International Journal of Gynecological Cancer*, vol. 32, no. 3. 2022. doi: 10.1136/ijgc-2021-003056.

[8] H. Hu *et al.*, "Deep learning applications in automatic segmentation and reconstruction in CT-based cervix brachytherapy," *J Contemp Brachytherapy*, vol. 13, no. 3, pp. 325–330, 2021, doi: 10.5114/JCB.2021.106118.

[9] X. Tian *et al.*, "Artificial intelligence in brachytherapy for cervical cancer," *Journal of Cancer Research and Therapeutics*, vol. 18, no. 5. 2022. doi: 10.4103/jcrt.jcrt_2322_21.

[10] J. Z. Zhao *et al.*, "Artificial intelligence applications in brachytherapy: A literature review," *Brachytherapy*, vol. 22, no. 4. 2023. doi: 10.1016/j.brachy.2023.04.003.

[11] S. Miller, J. Bews, and W. Kinsner, "Brachytherapy cancer treatment optimization using simulated annealing and artificial neural networks," *Canadian Conference on Electrical and Computer Engineering*, vol. 1, 2001, doi: 10.1109/CCECE.2001.933760.

[12] D. Zhang, Z. Yang, S. Jiang, Z. Zhou, M. Meng, and W. Wang, "Automatic segmentation and applicator reconstruction for CT-based brachytherapy of cervical cancer using 3D convolutional neural networks," *J Appl Clin Med Phys*, vol. 21, no. 10, 2020, doi: 10.1002/acm2.13024.

[13] A. A. Taha and A. Hanbury, "Metrics for evaluating 3D medical image segmentation: Analysis, selection, and tool," *BMC Med Imaging*, vol. 15, no. 1, 2015, doi: 10.1186/s12880-015-0068-x.

[14] F. Milletari, N. Navab, and S. A. Ahmadi, "V-Net: Fully convolutional neural networks for volumetric medical image segmentation," in *Proceedings - 2016 4th International Conference on 3D Vision, 3DV 2016*, 2016. doi: 10.1109/3DV.2016.79.

[15] P. Zaffino *et al.*, "Fully automatic catheter segmentation in MRI with 3D convolutional neural networks: Application to MRI-guided gynecologic brachytherapy," *Phys Med Biol*, vol. 64, no. 16, 2019, doi: 10.1088/1361-6560/ab2f47.

[16] H. H. Chang, A. H. Zhuang, D. J. Valentino, and W. C. Chu, "Performance measure characterization for evaluating neuroimage segmentation algorithms," *Neuroimage*, vol. 47, no. 1, 2009, doi: 10.1016/j.neuroimage.2009.03.068.

[17] L. J. Isaksson *et al.*, "Automatic Segmentation with Deep Learning in Radiotherapy," *Cancers*, vol. 15, no. 17. 2023. doi: 10.3390/cancers15174389.

[18] C. Janiesch, P. Zschech, and K. Heinrich, "Machine learning and deep learning," *Electronic Markets*, vol. 31, no. 3, 2021, doi: 10.1007/s12525-021-00475-2.

[19] O. Ronneberger, P. Fischer, and T. Brox, "U-net: Convolutional networks for biomedical image segmentation," in *Lecture Notes in Computer Science (including subseries Lecture Notes in Artificial Intelligence and Lecture Notes in Bioinformatics)*, 2015. doi: 10.1007/978-3-319-24574-4_28.

[20] A. Krizhevsky, I. Sutskever, and G. E. Hinton, "ImageNet classification with deep convolutional neural networks," *Commun ACM*, vol. 60, no. 6, 2017, doi: 10.1145/3065386.

[21] Y. Zhang *et al.*, "Multi-needle Localization with Attention U-Net in US-guided HDR Prostate Brachytherapy," *Med Phys*, vol. 47, no. 7, 2020, doi: 10.1002/mp.14128.

[22] Varian, "Brachytherapy Applicators & Accessories," *Varian Medical Systems*. 2018.

[23] T. P. Hellebust *et al.*, "Recommendations from Gynaecological (GYN) GEC-ESTRO working group: Considerations and pitfalls in commissioning and applicator reconstruction in 3D image-based treatment planning of cervix cancer brachytherapy," *Radiotherapy and Oncology*, vol. 96, no. 2, 2010, doi: 10.1016/j.radonc.2010.06.004.

[24] A. A. C. De Leeuw, M. A. Moerland, C. Nomden, R. H. A. Tersteeg, J. M. Roesink, and I. M. Jürgenliemk-Schulz, "Applicator reconstruction and applicator shifts in 3D MR-based PDR brachytherapy of cervical

cancer," *Radiotherapy and Oncology*, vol. 93, no. 2, 2009, doi: 10.1016/j.radonc.2009.05.003.

[25] K. Tanderup *et al.*, "Consequences of random and systematic reconstruction uncertainties in 3D image based brachytherapy in cervical cancer," *Radiotherapy and Oncology*, vol. 89, no. 2, 2008, doi: 10.1016/j.radonc.2008.06.010.

[26] J. Schindel, W. Zhang, S. K. Bhatia, W. Sun, and Y. Kim, "Dosimetric impacts of applicator displacements and applicator reconstruction-uncertainties on 3D image-guided brachytherapy for cervical cancer," *J Contemp Brachytherapy*, vol. 5, no. 4, 2013, doi: 10.5114/jcb.2013.39453.

[27] A. Lekatou, V. Peppa, P. Karaiskos, E. Pantelis, and P. Papagiannis, "On the potential of 2D ion chamber arrays for high-dose rate remote afterloading brachytherapy quality assurance," *Phys Med Biol*, vol. 67, no. 8, 2022, doi: 10.1088/1361-6560/ac612d.

Lingyun Qiu. (F'89) was born in Fuzhou, China. He embarked on his academic journey by pursuing a Bachelor of Engineering in Biomedical Engineering at East China University of Technology, graduating in June 2011. Driven by his passion for medical technology, he furthered his education with a Master of Engineering, focusing on the same field at South China University, earning his degree in June 2014.

He has dedicated his career to the field of radiotherapy, currently holding the position of Radiotherapy Engineer at the Zhejiang Provincial People's Hospital since August 2014. His work has been marked by significant contributions to clinical research, notably in the development of intelligent radiotherapy organ delineation using deep reinforcement learning artificial intelligence. His research endeavors have been supported by prestigious programs such as the Zhejiang Basic Public Welfare Research Program and the Zhejiang Medical and Health Science and Technology Program.

In addition to his professional achievements, Lingyun has authored several publications, including articles on 4D dosimetric evaluation technology for moving tumor radiotherapy plans. His current research interests lie in advancing radiotherapy treatment planning and the application of AI in medical imaging.

Rong Wu. was born in Wanzhi, Wuhu, Anhui, China in 1988. He received the B.S. degree in nurseing from the Southern Anhui Medical College.

She devoted his career to the field of Traditional Chinese medicine nursing and has been serving as a nurse at Hangzhou Hospital of Traditional Chinese Medicine since August 2012.

Xinpeng Lin(F'01)**.** was born in Hangzhou, China in 2001. He began his academic journey by pursuing a bachelor's degree in applied Physics at Hangzhou Medical College, graduating in June 2024.

During his undergraduate studies, he and his supervisor conducted in-depth research on Study on the reconstruction method of metal source donor in the afterloading treatment of cervical cancer based on U-net neural network and achieved some very good results. He will go to Wenzhou Medical University after his gradution as a graduate student in biomedical engineering and continue to engage in the research of artificial intelligence in biomedicine.

Lifeng Qiu. (M'01) was born in Guigang, China. She began her academic journey by pursuing a bachelor's degree in applied Physics at Hangzhou Medical College, graduating in June 2023. During her undergraduate studies, she and her supervisor conducted in-depth research on the four-dimensional dosimetry evaluation of exercise-based tumor radiotherapy programs and achieved some very good results. She has been working in the field of radiation therapy since her graduation and is currently working as a radiation therapy technician at Guangxi Medical University Kaiyuan Langdong Hospital. Her work has made significant contributions to clinical research, particularly in psychological interventions for young children and radiotherapy without anesthesia, as well as in the precise positioning and administration of radiotherapy under the TOMO knife.

Kainan Shao. (F'85) is a dedicated professional in oncological radiotherapy with a strong background in medical physics. He obtained his Bachelor of Engineering from Zhejiang University in 2007 and a Ph.D. in Medical Physics from the same university in 2012. Since August 2023, he has been working as a Radiotherapy Physics Specialist in the Department of Radiotherapy at Zhejiang Provincial People's Hospital. Before that, from July 2014 to July 2023, he served as a Radiotherapy Physics Specialist at Zhejiang Cancer Hospital. He has also been the principal investigator of the "Semi-Automatic Management Toolset for Radiotherapy Planning Based on RayStation Platform" project funded by the Zhejiang Provincial Medical and Health Science and Technology Plan, which has been successfully completed. With extensive knowledge and experience in radiotherapy physics, Shao Kainan has made significant contributions to the advancement of oncological treatment through his commitment to research and clinical practice, thereby enhancing patient care in radiotherapy.

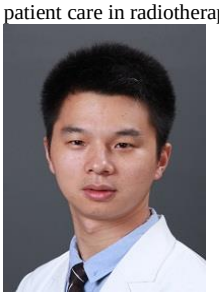

Wenming Zhan (F'83) was born in Linhai, Zhejiang Province, China. He graduate in Nuclear Engineering and Technology from Nanhua University. Since August 2007, He has been working in the Radiotherapy Department at Zhejiang Provincial People's Hospital With over a decade of experience in the field, he specializes in radiotherapy physics, focusing on tumor radiotherapy dosimetry, radiation dose measurement, and intensity-modulated radiotherapy technology. He has been

recognized for his expertise and has served as a committee member in various professional organizations, including the Zhejiang Provincial Anti-Cancer Association, the Chinese Biomedical Engineering Society, and the Zhejiang Provincial Biomedical Society.

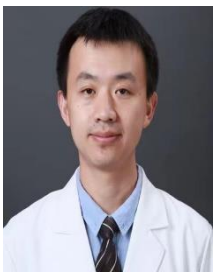

Qiang Li. (F'83) was born in Tai'an, China. In August 2003, he pursued a Bachelor's degree in Medical Imaging at Shandong First Medical University. He graduated in July 2008 and began his academic journey. Driven by his passion for medicine, he continued his studies at Shandong First Medical University, focusing on the same field and obtaining a Master's degree in Radiology Medicine in July 2019. He devoted his career to the field of radiation therapy and has been serving as a radiation therapist at Zhejiang Provincial People's Hospital since August 2008. His work has made significant contributions to clinical research, particularly in improving the accuracy of radiotherapy through the use of new technologies such as respiratory gating and stereotactic radiotherapy. He has participated in multiple projects such as the Zhejiang Provincial Natural Science Foundation and the Zhejiang Provincial Medical and Health Science and Technology Plan.

Jieni Ding. (M'83) was born in Zhejiang, China in 1999. She graduated from Hangzhou Medical College, majoring in Applied Physics, and obtained her Bachelor's degree in June 2022. During her undergraduate internship, she worked with her mentor on research related to Dosimetry and lung volume change in left breast cancer deep inspiratory breath holding with optical body surface positioning system, achieving certain results. After graduation, she has been continuously engaged in radiotherapy work and currently holds the position of medical physicist in the Radiotherapy Department of Zhejiang Provincial People's Hospital. Her job involves designing treatment plans to ensure the safety of patients undergoing radiotherapy, allowing them to safely receive precise radiotherapy. In addition, she also participates in the daily checks of the treatment equipment to ensure its stability, accuracy, and safety.

Yucheng Li. (F'91) was born in Tai'an, China. He primarily specializes in the fields of artificial intelligence and oncological radiotherapy. He serves as a Radiotherapy Physics Specialist in the Department of Radiotherapy at Zhejiang Provincial People's Hospital and holds a Master's degree from the University of South China. He is also a committee member of the Radiotherapy Physics Technical Group under the Zhejiang Provincial Anti-Cancer Association and the Young Committee member of the Tumor Radioactive Particle and Nutrition Intelligent Diagnosis and Treatment Special Committee under the Zhejiang Provincial Mathematical Medicine Society. With three SCI papers published, he was awarded first prize in the planning competition held by the Zhejiang Provincial Anti-Cancer Association's Radiotherapy Physics Technology Association in 2022.

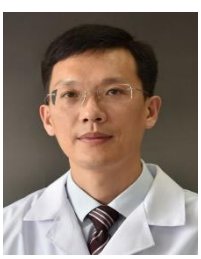

Weijun Chen. (F'78) was born in yuyao, China. He has established himself as a leading figure in the field of radiotherapy. He obtained his Bachelor of Engineering in South China University, Hengyang, Hunan, China, in July 2000, and furthered his education with a Bachelor of Medicine from Wenzhou Medical College, Wenzhou, Zhejiang, China, in June 2010. He completed his Master of Engineering at Tsinghua University, Beijing, Beijing Municipality, China, in January 2011, majoring in lower-cased field of study.

He has accrued extensive experience in radiotherapy, beginning his career as the Deputy Director of the Radiotherapy Physics Department at Zhejiang Cancer Hospital from August 2000 to July 2017. Since August 2017, he has served as the Deputy Director and Senior Radiotherapy Engineer at Zhejiang Provincial People's Hospital. His research has been influential, with his work on "Intelligent Delineation of Organs at Risk in Radiotherapy using Deep Reinforcement Learning AI" and "4D Dosimetric Evaluation Technology for Moving Tumor Radiotherapy Plans" being recognized by the Zhejiang Basic Public Welfare Research Program and the Zhejiang Medical and Health Science and Technology Program. He has also completed a significant study on "Correlation between Radioactive Brain Injury after Nasopharyngeal Carcinoma Radiotherapy and the Volume Dose of Irradiated Brain Tissue."

He is actively involved in professional societies and has been recognized with numerous awards for his contributions to the field. His commitment to advancing radiotherapy and medical engineering is evident through his service on various committees and publications.